This article has been accepted for publication in a future issue of this journal, but has not been fully edited. Content may change prior to final publication. Citation information: DOI 10.1109/LMAG.2016.2615852, IEEE Magnetics Letters

Magnetochemistry

Instability-Induced Mixing of Ferrofluids in Uniform Magnetic Fields

Xinghua Wang[1], Zhaomeng Wang[1], Vijaykumar B. Varma[1], Zhiping Wang[2], Ayan Ray[1], W. S. Lew[3], and R. V. Ramanujan[1*]

[1]School of Materials Science and Engineering, Nanyang Technological University, Singapore, 639798.
[2]Singapore Institute of Manufacturing Technology, 71 Nanyang Dr, Singapore 638075.
[3]School of Physical and Mathematical Sciences, Nanyang Technological University, Singapore, 637371.
*Member, IEEE

Abstract- The advantages of ferrofluids in microfluidic lab-on-a-chip applications include remote control of the fluid flow within the chips, e.g., mixing of the species using an external uniform magnetic field. Hence, three-stream flow systems, consisting of a ferrofluid core clad by two streams of diamagnetic silicone oil were studied. The instability of the ferrofluid, subjected to an external uniform magnetic field, was studied. When the strength of this magnetic field was increased to a critical value, the ferrofluid was spread toward the silicone oil and a transient instability developed at the ferrofluid-silicone oil interface. Further increasing magnetic field resulted in periodic instability structures and permanent instability. The effect of magnetic field strength, flow rate and flow rate ratio were determined. With a higher flow rate ratio, the permanent instability was observed only at the larger magnetic field strength. Our modeling results were consistent with these experimental results. Our work shows that an external uniform magnetic field of only a few millitesla can lead to instability and mixing, thus it is relevant to mixing in practical microfluidic devices.

Index Terms- Magnetochemistry, micro-magnetofluidics, ferrofluid instability, LoC mixing, uniform magnetic fields, microfluidics.

I. INTRODUCTION

Microfluidics relates to a set of technologies for accurate control of fluid flow in the volume range µl to pl for different Lab-on-a-Chip (LoC) applications, e.g. drug discovery[Neuzi 2012], biochemical assay[Haeberle 2007], blood analysis[Toner 2005], and biological cells[Yi 2006]. One of the most important aspects of fluidic devices is mixing[Suh 2010, Ward 2015]. When the channel size is in the micron range, laminar flow is observed due to the low Reynolds number, and diffusion is the main mixing mechanism[Ward 2015]. Hence, controlled mixing of the species in microchannels is a challenge[Garoosi 2015]. To enhance the mixing, various methods have been employed[Ding 2013, Ward 2015], mainly categorized as passive and active mixing. Passive mixing was performed by long microchannels[Eskin 2012], specific geometrical features[Zhu 2012c], serpentine mixers[Afzal 2014], zigzag mixers[Afzal 2013], and patterned blocks[Jeon 2009]. The difficulty in these passive schemes is the complex and expensive microchannel fabrication with specific geometric features.

The active mixing method performs controlled mixing by generating chaotic flow patterns using mechanical forces[Tierno 2007] and electrical forces[Sugioka 2010]. Active mixing, in practice, is limited for electric, mechanical and acoustic methods [Ward 2015] due to the need of integrated electrodes, moving parts and a bubble or air interface, respectively. Such integration requires complex designs and fabrication techniques. Undesirable temperature increase by applied electric, optical or acoustic fields[Evander 2007] is unsuitable for cells or deoxyribonucleic acids (DNA) [Selva 2010]. This describes need of a technology that is low cost, simple, and wireless with no heat generation to enable mixing in microfluidic systems.

A micromagnetofluid (µMF) system[Wang 2015a, Wang 2015b, Varma 2016, Wang 2016], which is a microfluidic platform integrated with the magnetic field and magnetic fluid is advantageous for LoC based mixing applications. Few studies have been reported for µMF mixing in the ferrohydrodynamic (FHD) regime, e.g., (i) a serpentine design with a non-uniform magnetic field[Zolgharni 2007], (ii) FHD pumping with a traveling magnetic field[Mao 2011]. The advantages µMF on a LoC platform were not fully explored by the non-uniform magnetic field because (i)larger magnets or coils are required to generate substantial gradient force[Sander 2012, Zeng 2013];(ii) magnetic field gradients are sensitive to the location of the magnets[Pankhurst 2003, Pamme 2006]; and (iii) complex fabrication techniques are required to integrate the microcoils[Beyzavi 2009].

On the other hand, *a uniform magnetic field (H)* offers a convenient implementation of the µMF technique for programmable and wireless LoC mixing by inducing various types of instabilities in the FHD regime. Rosensweig[Rosensweig 2013] investigated various types of instabilities in the FHD regime. In the literature, various studies of FHD instabilities were performed under the influence of uniform magnetic field H, such as (i) hybrid FHD instability[Chen 2008]; (ii) planar, spiral and three-dimensional[Belyaev 2010]; (iii) FHD pattern formation[Zakinyan 2016]; and (iv) theoretical investigations of pattern formation[Richardi 2004].

A uniform magnetic field on a LoC platform can give rise to interesting new types of *µMF instability*, termed as magnetofluidic spreading[Zhu 2012a], which can be useful for LoC based mixing[Zhu 2012b]. In our previous work[Wang 2015a, Wang 2015b], Wang et al. investigated the spreading of the ferrofluid core stream (clad by a miscible fluid) in the presence of a *uniform magnetic field*. Control of the magnetofluidic spreading was described,

Corresponding author: R. V. Ramanujan (ramanujan@ntu.edu.sg)

This article has been accepted for publication in a future issue of this journal, but has not been fully edited. Content may change prior to final publication. Citation information: DOI 10.1109/LMAG.2016.2615852, IEEE Magnetics Letters

concluding that the dominant effect was due to cross-sectional convection induced by the magnetic forces[Wang 2015a]. It is evident from the literature that uniform magnetic field induced μMF instability on a LoC platform has not yet been investigated in detail.

This work reports an investigation of the magnetically induced ferrofluid instability in a three stream fluid system: oil based ferrofluid as the core stream, clad by silicone oil streams, with specific flow and field parameters. We found that by tuning parameters such as the field H, the ferrofluid laminar flow (FLF) undergoes a ferrofluid transient instability (FTI), ferrofluid permanent instability (FPI) and finally reaches μMF spreading (μMFS). The μMFS can be classified as a special case of instability. The magnetic field produces a force acting on the magnetic nanoparticles (MNP) in the ferrofluid, changing the particle concentration profile. A range of ferrofluid flow rates (Q_{ff}) and flow rate ratios (Φ) was utilized to map the instability. The significance of our work is that a uniform magnetic field of only a few mT can lead to substantial instability and mixing. We have recently demonstrated the use of such a wireless, programmable LoC mixing platform for magnetically trapping bacteria[Wang 2016]. The present studies are an extension of our earlier work to demonstrate a wirelessly controlled LoC mixing platform activated at low magnetic fields[Wang 2016], which can be useful for combinatorial mixing[Tani 2015], cell analysis[Occhetta 2016], biofluid capture[Scherr 2016], biosensing [Luka 2015], bioassay[van Reenen 2014], DNA hybridization[Raynal 2013], liposomes self-assembly[Kennedy 2012], determination of cell metabolites[Lin 2016] and synthesis of gradient hydrogels[Mahadik 2014].

II. MATERIALS AND EXPERIMENTAL METHODS

Commercially available silicone oil (Shin-Etsu, Japan) and oil-based ferrofluid (EMG 909, FerroTec, Singapore) were employed. The measured viscosity and density of EMG 909 are (3.02±0.01) mPa.s and (1.022±0.003) $\times 10^3$ kg/m^3, respectively. The properties of EMG 909 provided from the supplier datasheet are saturation magnetization of 22 mT, the initial magnetic susceptibility of 1.38, the particle diameter of 10nm, and MNP volume concentration of 3.9 %. Silicone oil with a viscosity of η_o=(23.6±0.03) mPa·s and a density of ρ_o=(0.838±0.002) $\times 10^3$ kg/m^3 was used.

The microchip was made from poly(methyl methacrylate) by standard micro-milling techniques, followed by thermal bonding[Wang 2015b]. The test channel has three inlets and two outlets (the dimensions are given in Fig.1a). A Phantom MIRO high-speed camera (M320S) was utilized for imaging. A dual rate syringe pump (KDS Gemini 88) was used to drive fluid flow into the chip. A DEXING electromagnet (DXSB-178) was used to generate a uniform magnetic field H, with a 5 cm air gap between the two parallel poles (pole face diameter of 7.5 cm).

III. NUMERICAL MODELING

A two-dimensional (2D) numerical simulation was performed with the experimental channel dimensions (Fig.1a). A fully developed average velocity profile $\bar{u}$ was assumed and calculated for the inlet flow rate Q_{IL}, the width W, and the depth D of the channel using the formula

$$\bar{u}=Q_{IL}/WD \quad (1)$$

The no-slip condition with the initial flow conditions, u=0 m/s and P= 0 Pa were used. The equation of motion for an unsteady, viscous and incompressible system[Rosensweig 2013, Wang 2015a, Wang 2015b, Varma 2016] was defined by:

$$\rho\, \partial\boldsymbol{u}/\partial t + \rho(\boldsymbol{u}\cdot\nabla)\mathbf{u} = \boldsymbol{\nabla}\cdot[-P + \eta(\nabla\mathbf{u} + (\nabla\boldsymbol{u})^{\boldsymbol{T}})] + \boldsymbol{F_m} \quad (2)$$

$$\partial\rho/\partial t + \nabla\cdot(\rho\boldsymbol{u}) = 0 \quad (3)$$

where ρ, $\boldsymbol{u}$, η, P and $\boldsymbol{F_m}$ are the fluid density, velocity vector, viscosity, pressure, and the magnetic volume force, respectively. The interfacial tension and gravitational force were neglected because it is a miscible fluid system at the micro-scale.

The distribution of the MNP concentration (C) in the microchannel with the velocity vector $\boldsymbol{u_p}$, was defined by the transport equation[Zhu 2012a, Wang 2015a, Wang 2015b]:

$$\partial C/\partial t + (\boldsymbol{u_p}\cdot\boldsymbol{\nabla})C = D\nabla^2 C \quad (4)$$

where, $D=k_BT/6\pi\eta r_p$ is diffusivity at temperature T and MNP radius r_p. k_B is Boltzmann's constant The velocity vector was defined by the Stokes drag relationship[Wang 2015a, Wang 2015b]:

$$\boldsymbol{u_p} = \boldsymbol{u} + \boldsymbol{u_{mag}} \quad (5)$$

where $u_{mag} = F_{mag}/6\pi\eta r_p$ is the particle drift velocity due to magnetic force $\boldsymbol{F_{mag}}$ [Nguyen 2012, Zhu 2012a, Wang 2015a, Wang 2015b], defined by:

$$\boldsymbol{F_{mag}} = (1\backslash 2)V_p\mu_0\nabla\chi\boldsymbol{H^2} \quad (6)$$

where V_p is the MNP volume, $\chi=\chi_m C$ is the susceptibility of the mixed fluid, μ_0 is permeability of free space. The magnetic field $\boldsymbol{H}=\boldsymbol{B}/\mu_0$ (H<saturation magnetization of 22 mT) was applied along the y direction(Fig.1a). Magnetic field was defined by the Maxwell equation. In a simply connected domain with no free current

$$\nabla\times\boldsymbol{H} = 0 \quad (7)$$

The magnetic scalar potential ψ ($\boldsymbol{H}$ =-$\nabla\psi$) was introduced to determine the magnetic force. χ was assumed to vary linearly with particle concentration. The magnetic potential equation for field H was defined by [Pankhurst 2003]:

$$\nabla\cdot[(1+\chi)\nabla\psi] = 0 \quad (8)$$

and the corresponding magnetic force can be expressed as[Zhu 2012a]:

$$\boldsymbol{F_m} = -(1/2)\mu_0|\boldsymbol{H}|^2 C_V\nabla\chi \quad (9)$$

Where $C_V = C_{V0}C$, is the volume concentration of the particles with an initial particle volume concentration of C_{V0} = 0.04. The non-dimensional volume concentration C was determined by Eq. (4). The boundary condition for the magnetic field is:

$$\boldsymbol{H}\cdot\boldsymbol{\hat{n}} = -\boldsymbol{\partial\psi/\partial n}, \forall x \in \partial\psi \quad (10)$$

Where, $\boldsymbol{\hat{n}}$ is the unit vector normal to the surface. The density and viscosity for the fluid concentration (C)[Zhu 2012b, Wang 2015a, Wang 2015b] were defined as:

$$\rho = C\rho_m + (1-C)\rho_0 \quad (11)$$

$$\eta = \eta_m\exp(R(1-C)) \quad (12)$$

Where ρ_m and ρ_0 are the densities of ferrofluid and silicone oil, respectively. The viscosity parameter (R) for the ferrofluid viscosity (η_m) and silicone oil viscosity (η_o) was defined by $R = \ln(\eta_o/\eta_m)$.

Simulations of the magnetic field distribution, velocity field, and concentration field were performed by the finite-element methods in COMSOL™ software. The mesh was defined by a free triangular method with total 26100 domain elements (with a minimum and an average element quality of 0.33 and 0.90, respectively).

IV. RESULTS

Under the influence of a magnetic field H, the ferrofluid core

This article has been accepted for publication in a future issue of this journal, but has not been fully edited. Content may change prior to final publication. Citation information: DOI 10.1109/LMAG.2016.2615852, IEEE Magnetics Letters

stream flow can exhibit instabilities, such as FTI, FPI, and μMFS. The effect of H leading to these instabilities, the time dependence of the instabilities, the effect of Q_{ff}, and Φ are described in the following subsections. Where, $\Phi=Q_{oil}/Q_{ff}$, is the ratio of flow rate between oil cladding (Q_{oil}) and core streams (Q_{ff}). A critical magnetic field H_c, defined as the minimum required magnetic field to observe the specific instability, was used to modulate the transition from one type of flow to the other.

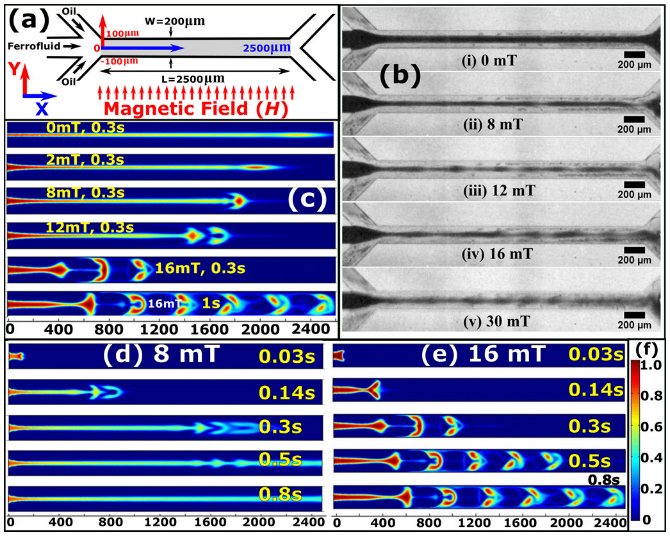

Fig.1: **(a)** Schematic of chip design[Zhu 2012a, Wang 2015a, Wang 2015b]. The flow and the applied uniform magnetic field (H) are in x and y-direction, respectively. The shaded region from (0,-100)μm to (2500, 100)μm is the area of interest. The microchannel depth is D= 50 μm. **(b-c)** FTI and FPI at Q_{ff} = 50μl/h, Φ = 3: (b) experiments, after 2 min flow, (c) simulations. For H≤2 mT, laminar flow can be observed in both the experiments and the simulations. The FTI can be observed only in the simulations for 2 mT<H≤12 mT. The FPI was observed at H≥12 mT in the experiments and H≥ 16 mT in the simulations. **(d-e)** Simulations at time 0.03s to 0.8s: (d) FTI at 8 mT, (e) FPI at 16 mT. **(f)** Color bar showing volume fraction (VF) of the ferrofluid core for the simulated results of (c-e). The red indicates VF=1 (ferrofluid) and blue indicates VF=0 (silicone oil). Intermediate VFs are indicated by: light blue=0.2, cyan=0.4, yellow=0.6 and orange=0.8.

A. Effect of a uniform magnetic field

Figure 1b shows experimental micrographs of the μMF instability at different field H, for Q_{ff} equal to 50μl/h and Φ equal to 3. The results clearly show (Fig.1b) that, without the magnetic field, the ferrofluid core clad by the silicone oil exhibits FLF. The ferrofluid core began to spread into the silicone oil with increasing H due to the migration of the MNPs under the influence of the magnetic force. At 8 mT, significant spreading of ferrofluid core was observed, followed by undulation along the channel length. At 12 mT, periodic branches of the permanent instability were observed, which does not vanish with time. Increasing of H to 16 mT, increases the width of the instability branch, and the longitudinal spacing between branches was also increased. When the H increased above 30 mT, the ferrofluid core began to mix with the silicone oil, significantly disrupting the flow.

Figure 1b and 1c compare the experiments and simulations for the instabilities. From the simulations, the *FTI* was observed at 8 mT (Fig.1c), and this appears only for a short time at the "stream-head" section when the ferrofluid core enters in the channel which contains silicone oil. Experimentally, the FTI could not be captured; there was an overlap of flow instabilities due to the unsteady states of the syringe pump that occurs for up to 2 min after the pump was switched on, which is longer than the time at which FTI is predicted to occur.

In the simulations, the FPI required at a magnetic field of 16 mT, which is higher than the experimental value of 12 mT. This lower experimental value of 12 mT for producing the FPI may be due to inter-particle interactions of the MNPs, e.g. chain formation. Hence, the difference between the model and experiment may be due to the continuum approximation used in our micro-magnetofluidic numerical model, which does not consider inter-particle interactions of the MNP[Rosensweig 2013].

B. Time dependence of instability

Time-dependent numerical simulations were performed to study the FTI and the FPI of the ferrofluid core in the silicone oil cladding. The FTI was observed at a critical field H_c of 8 mT (Fig.1d), and starts at 0.03 s of the ferrofluid core flow. The FTI vanishes at 0.8 s followed by the FLF. At high H ferrofluid instability developed at the beginning of the flow which does not decay with time and leads to the *FPI*. At 16 mT, a FPI (Fig.1e) appears at 0.14 s as the ferrofluid enters into the microchannel. As time and the ferrofluid flow progress, the FPI patterns start filling the channel and remain for the duration of the simulations.

C. Effect of flow rate and flow rate ratio

Experimental investigations (Figure 2c) were performed at Q_{ff} of 25, 50, 75 μl/h, Φ of 1, 2, 3 and at different H_c to understand its effect on the FPI. As shown in Fig.2c, H_c increases linearly with increasing Q_{ff}. For a constant Q_{ff} 75μl/h, the H_c increases linearly with the Φ. For lower Q_{ff} (25 and 50μl/h) the H_c shows a slower increase with increasing Φ. Increasing the Φ lead to an increase in the hydrodynamic focusing[Knight 1998]. The increase in the convective diffusion and the particle drift velocity ($\boldsymbol{u_p}$) opposes the hydrodynamic focusing, leading to the FPI. Convective diffusion and $\mathbf{u_p}$ decrease with increasing Q_{ff} and increases with increasing H [Wang 2015a]. The H_c increases with increasing Q_{ff} and increasing Φ.

D. Instability Map

The present work used Q_{ff}, Φ and H to quantify the transition from FLF to the different instabilities i.e., (i) FTI (ii) FPI and (iii) μMFS. μMFS has been reported earlier[Zhu 2012a, Wang 2015a, Wang 2015b], but the other types of instabilities were not previously described. The variation number (VN) was defined to obtain a dimensionless number, by normalizing the maximum Q_{ff} value to 1.

$$\mathrm{VN}=(50\ \mu\mathrm{l/h})/Q_{ff} \tag{13}$$

Figure 2a and 2b shows the instability map based on the VN, and consists of the regions of FLF, FTI, FPI and μMFS. Figure 2a shows an instability map for a constant Φ =2. The FTI is the first transition from the FLF, induced by the increase in the H or the increase in the VN (i.e. decrease in Q_{ff}). At lower H, the FTI was observed at all Q_{ff} values. The FTI turned into a FPI for H higher than 3 mT or VN higher than 2. The FPI exist in certain regions of the instability map specific to the combination of VN and magnetic field H, as denoted by the circular points. The FPI turns into μMFS for H greater than 4 mT, exhibiting μMFS patterns similar to those reported in our previous work[Wang 2015a, Wang 2015b]. The μMFS was observed for VN equal to 4 at 4mT and for VN greater than 1 at 6 mT.

Figure 2b shows the effect of Φ on the instability at a constant magnetic field of 3.6 mT. The FTI was observed at all Φ for VN≤ 2,

This article has been accepted for publication in a future issue of this journal, but has not been fully edited. Content may change prior to final publication. Citation information: DOI 10.1109/LMAG.2016.2615852, IEEE Magnetics Letters

except for VN=2, Φ=2. At VN=2.5 a transition in the instability from FTI to FPI and then from FPI to the spreading was observed with decreasing Φ. At Φ=2, μMFS was observed for VN≥2.5.

Thus, a combination of *H*, Φ and Q_{ff} is needed to induce instabilities and their magnitude defines the type of instability.

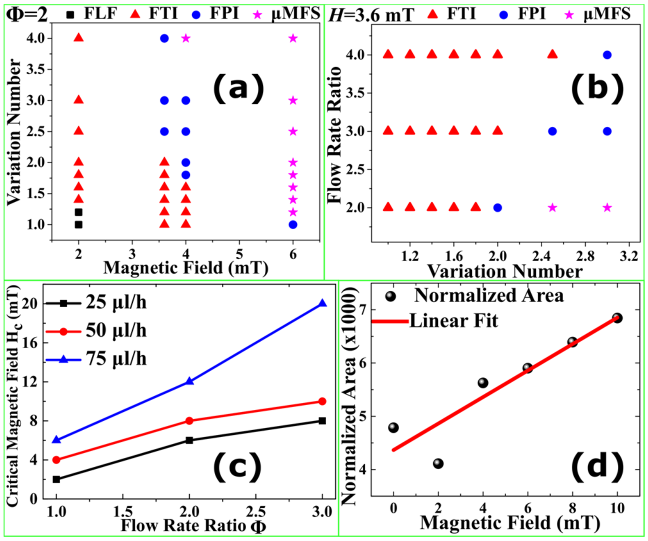

Fig.2: **(a-b)** Instability map, showing the dependence of FLF, FTI, FPI, μMFS on *H*, Φ and VN at (a) Φ=2 (b) *H*=3.6 mT where VN=(50μl/h)/Q_{ff}. **(c)** Critical magnetic field (H_c) required to induce FPI at different Φ and Q_{ff}=25, 50,75 μl/h. (d) The normalized area under the curve (higher value indicates more mixing) for different *H,* for the ferrofluid concentration profiles of Fig.3b.

V. DISCUSSION

The instabilities (FTI, FPI or μMFS) are a result of competition between hydrodynamic focusing[Knight 1998], convective diffusion, and particle drift velocity[Wang 2015a]. The hydrodynamic focusing increases with Φ and η_o. The convective diffusion due to the local fluid velocity depends on (i) the inflow conditions: Q_{ff}, channel geometry, viscosity and (ii) the velocities due to $\boldsymbol{F_m}$. The force $\boldsymbol{F_m}$ depend on *H*, χ_m and $\nabla\chi$**.** The gradient $\nabla\chi$ exists due to variation in MNP concentration from the core to the cladding. The particle drift velocity is defined by $\boldsymbol{u_{mag}}$, which depends on *H*, r_p, χ_m and viscosity.

The dominance of the hydrodynamic focusing results in FLF[Knight 1998]. The dominance of the convective diffusion or $\boldsymbol{u_{mag}}$ results in μMFS [Wang 2015a, Wang 2015b]. The intermediate state leads to either FTI or FPI.

VI. APPLICATION TO MIXING

The applicability of the present work was demonstrated by the mixing of the ferrofluid core and the silicone oil cladding induced at low *H* (*H* ≤ 10 mT). The experiments and the simulations were performed for *H* ranging from 0 to 10 mT, at a Φ of 3 and for a Q_{ff} of 25 μl/h. Figure 3a shows the experimental micrographs of mixing and Fig.3(b-c) shows the results of the quantitative experiments and the simulation results for the ferrofluid concentration profile (FCP). The FCP (Fig.3b-c) was determined by measuring the corrected mean gray values of 2500μm×200μm area (shaded region in Fig.1a) using ImageJ software. The corrected mean gray value was then normalized with respect to the maxima at *H*=0 mT (Fig.3a, 3b), which is the maximum of the FCP; the FCP (in %) was obtained in ±y direction (Fig.1a). The width of the FCP (Fig.3b) indicates mixing of the ferrofluid with silicone oil. The mixing was quantified by calculating the normalized area under the curve (all curves were normalized to 100, the area under the curve was then measured) as shown in Fig.2d.

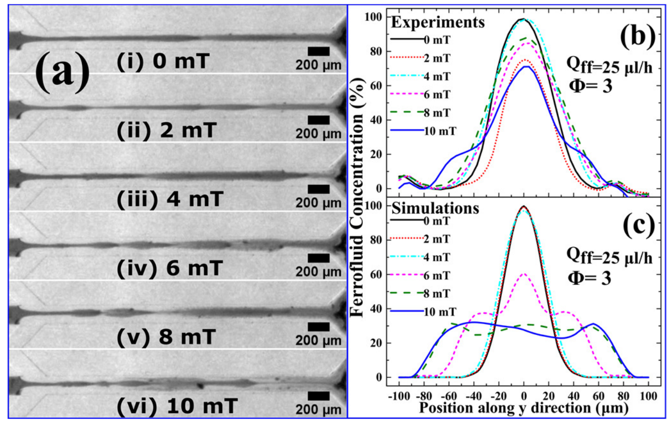

Fig.3: **(a)** Experimental micrographs of the mixing by the μMF instability for different *H*, after 2 min of ferrofluid flow. **(b-c)** Experimental results and the simulations showing the ferrofluid concentration profiles in ±y direction (y= -100 to 100 μm in Fig.1a), for low H (H ≤10 mT), Φ= 3 and Q_{ff}= 25 μl/h. (b) Experimental results after 2 min. (c) Simulation results after 30 s.

The experiments were performed for 2 min of ferrofluid flow (Fig.3a), where a significant change in the FCP was observed. For *H* less than 6 mT, the FCPs similar to that of 0 mT were observed. However, at a critical magnetic field of 6 mT, a significant increase in the width of the FCP (Fig.3b) can be observed, which increases with increasing *H* (Fig.2d). At 10 mT, the experimental FCP shows the widest distribution of the ferrofluid in ± y direction. The normalized area increases with the increasing *H* (Fig.2d), except for 2 mT. For 2 mT, focusing of the ferrofluid core focusing was observed, instead of mixing.

The simulations were performed for a flow time of 30 s where significant changes in the FCPs for the mixing were observed. The FCPs (in ±y direction) were obtained and normalized with respect to the maxima at 0mT (Fig.3c). It was found that when *H* was lower than the critical value of 6 mT, the MNPs were concentrated at the center, producing a peak in the FCP. For *H* less than 6 mT, no significant changes in the FCP were observed, similar to the experimental FCP. FPI occurred, at 6 mT, which is evident from the broadening of the FCP curve (Fig.3c), indicating significant migration of the MNPs into the silicone oil. For *H* greater than 6mT, the FCP shows the highest broadening, indicating fluid mixing. The numerical and experimental FCPs demonstrated similar trends in the mixing caused by magnetofluidic instability. The highest mixing was observed at 10 mT for both. However, in the simulations, significant mixing starts from 6 mT, while a similar mixing profile was observed at 10 mT in the experiments. This mismatch may have been caused due to the interparticle interactions which were not considered in our model.

Our experiments and simulations demonstrated substantial mixing at low H (*H* ≤ 10 mT). This μMF based wireless, programmable LoC mixing platform can be useful for magnetic trapping of bacteria[Wang 2016], biofluids capture[Scherr 2016], biosensing[Parks 2014, Luka 2015], and bioassay[van Reenen 2014].

ACKNOWLEDGMENT

This work was supported by the Science and Engineering Research Council (SERC), Singapore through A*STAR PSF 2012 Project: 1321202078.

REFERENCES

Afzal A, Kim K Y (2013), "Mixing performance of passive micromixer with sinusoidal channel walls," *Journal of Chemical Engineering of Japan,* vol. 46, pp. 230-238.

Afzal A, Kim K Y (2014), "Flow and mixing analysis of non-Newtonian fluids in straight and serpentine microchannels," *Chemical Engineering Science,* vol. 116, pp. 263-274.

Belyaev A, Smorodin B (2010), "The stability of ferrofluid flow in a vertical layer subject to lateral heating and horizontal magnetic field," *Journal of Magnetism and Magnetic Materials,* vol. 322, pp. 2596-2606.

Beyzavi A, Nguyen N T (2009), "One-dimensional actuation of a ferrofluid droplet by planar microcoils," *J Phys D Appl Phys,* vol. 42, 015004.

Chen C-Y, Tsai W-K, Miranda J A (2008), "Hybrid ferrohydrodynamic instability: Coexisting peak and labyrinthine patterns," *Physical Review E,* vol. 77, p. 056306.

Ding X Y, Li P, Lin S C S, Stratton Z S, Nama N, Guo F, Slotcavage D, Mao X L, Shi J J, Costanzo F, Huang T J (2013), "Surface acoustic wave microfluidics," *Lab on a Chip,* vol. 13, pp. 3626-3649.

Eskin D, Mostowfi F (2012), "A model of a bubble train flow accompanied with mass transfer through a long microchannel," *International Journal of Heat and Fluid Flow,* vol. 33, pp. 147-155.

Evander M, Johansson L, Lilliehorn T, Piskur J, Lindvall M, Johansson S, Almqvist M, Laurell T, Nilsson J (2007), "Noninvasive acoustic cell trapping in a microfluidic perfusion system for online bioassays," *Analytical Chemistry,* vol. 79, pp. 2984-2991.

Garoosi F, Rohani B, Rashidi M M (2015), "Two-phase mixture modeling of mixed convection of nanofluids in a square cavity with internal and external heating," *Powder Technology,* vol. 275, pp. 304-321.

Haeberle S, Zengerle R (2007), "Microfluidic platforms for lab-on-a-chip applications," *Lab on a Chip,* vol. 7, pp. 1094-1110.

Jeon W, Shin C B (2009), "Design and simulation of passive mixing in microfluidic systems with geometric variations," *Chemical Engineering Journal,* vol. 152, pp. 575-582.

Kennedy M J, Ladouceur H D, Moeller T, Kirui D, Batt C A (2012), "Analysis of a laminar-flow diffusional mixer for directed self-assembly of liposomes," *Biomicrofluidics,* vol. 6, 044119, p. 14.

Knight J B, Vishwanath A, Brody J P, Austin R H (1998), "Hydrodynamic focusing on a silicon chip: Mixing nanoliters in microseconds," *Physical Review Letters,* vol. 80, pp. 3863-3866.

Lin X X, Leung K H, Lin L, Lin L Y, Lin S, Leung C H, Ma D L, Lin J M (2016), "Determination of cell metabolite VEGF(165) and dynamic analysis of protein-DNA interactions by combination of microfluidic technique and luminescent switch-on probe," *Biosensors & Bioelectronics,* vol. 79, pp. 41-47.

Luka G, Ahmadi A, Najjaran H, Alocilja E, DeRosa M, Wolthers K, Malki A, Aziz H, Althani A, Hoorfar M (2015), "Microfluidics Integrated Biosensors: A Leading Technology towards Lab-on-a-Chip and Sensing Applications," *Sensors,* vol. 15, pp. 30011-30031.

Mahadik B P, Wheeler T D, Skertich L J, Kenis P J A, Harley B A C (2014), "Microfluidic Generation of Gradient Hydrogels to Modulate Hematopoietic Stem Cell Culture Environment," *Advanced Healthcare Materials,* vol. 3, pp. 449-458.

Mao L, Elborai S, He X, Zahn M, Koser H (2011), "Direct observation of closed-loop ferrohydrodynamic pumping under traveling magnetic fields," *Physical Review B - Condensed Matter and Materials Physics,* vol. 84, 104431.

Neuzi P, Giselbrecht S, Lange K, Huang T J, Manz A (2012), "Revisiting lab-on-a-chip technology for drug discovery," *Nat Rev Drug Discov,* vol. 11, pp. 620-32.

Nguyen N T (2012), "Micro-magnetofluidics: interactions between magnetism and fluid flow on the microscale," *Microfluidics and Nanofluidics,* vol. 12, pp. 1-16.

Occhetta P, Licini M, Redaelli A, Rasponi M (2016), "Design of a microfluidic strategy for trapping and screening single cells," *Medical Engineering & Physics,* vol. 38, pp. 33-40.

Pamme N (2006), "Magnetism and microfluidics," *Lab chip,* vol. 6, pp. 24-38.

Pankhurst Q A, Connolly J, Jones S K, Dobson J (2003), "Applications of magnetic nanoparticles in biomedicine," *Journal of Physics D: Applied Physics,* vol. 36, p. R167.

Parks J W, Olson M A, Kim J, Ozcelik D, Cai H, Carrion R, Patterson J L, Mathies R A, Hawkins A R, Schmidt H (2014), "Integration of programmable microfluidics and on-chip fluorescence detection for biosensing applications," *Biomicrofluidics,* vol. 8, 054111, p. 8.

Raynal F, Beuf A, Carriere P (2013), "Numerical modeling of DNA-chip hybridization with chaotic advection," *Biomicrofluidics,* vol. 7, 034107, p. 14.

Richardi J, Pileni M (2004), "Towards efficient methods for the study of pattern formation in ferrofluid films," *The European Physical Journal E,* vol. 13, pp. 99-106.

Rosensweig R E (2013), *Ferrohydrodynamics*: Dover Publications, Inc. New York.

Sander J S, Erb R M, Denier C, Studart A R (2012), "Magnetic transport, mixing and release of cargo with tailored nanoliter droplets," *Adv Mater,* vol. 24, pp. 2582-7, 2510.

Scherr T F, Ryskoski H B, Doyle A B, Haselton F R (2016), "A two-magnet strategy for improved mixing and capture from biofluids," *Biomicrofluidics,* vol. 10, 024118, p. 15.

Selva B, Miralles V, Cantat I, Jullien M C (2010), "Thermocapillary actuation by optimized resistor pattern: Bubbles and droplets displacing, switching and trapping," *Lab on a Chip - Miniaturisation for Chemistry and Biology,* vol. 10, pp. 1835-1840.

Sugioka H (2010), "Chaotic mixer using electro-osmosis at finite Péclet number," *Physical Review E,* vol. 81, p. 036306.

Suh Y K, Kang S (2010), "A Review on Mixing in Microfluidics," *Micromachines,* vol. 1, pp. 82-111.

Tani M, Kawano R, Kamiya K, Okumura K (2015), "Towards combinatorial mixing devices without any pumps by open-capillary channels: fundamentals and applications," *Scientific Reports,* vol. 5, 10263, p. 13.

Tierno P, Johansen T H, Fischer T M (2007), "Magnetically driven colloidal microstirrer," *The Journal of Physical Chemistry B,* vol. 111, pp. 3077-3080.

Toner M, Irimia D (2005), "Blood-on-a-chip," *Annual Review of Biomedical Engineering,* vol. 7, pp. 77-103.

van Reenen A, de Jong A M, den Toonder J M J, Prins M W J (2014), "Integrated lab-on-chip biosensing systems based on magnetic particle actuation - a comprehensive review," *Lab on a Chip,* vol. 14, pp. 1966-1986.

Varma V B, Ray A, Wang Z M, Wang Z P, Wu R, Jayaneel P J, Sudharsan N, Ramanujan R V (2016), "Controlling Ferrofluid Droplets in Microchannels by Uniform Magnetic Fields," *IEEE Magnetics Letters,* vol. 7, p. In Press.

Wang Z M, Varma V B, Wang Z P, Ramanujan R V (2015a), "Tuning magnetofluidic spreading in microchannels," *Journal of Micromechanics and Microengineering,* vol. 25, p. 124001.

Wang Z M, Varma V B, Xia H M, Wang Z P, Ramanujan R V (2015b), "Spreading of a ferrofluid core in three-stream micromixer channels," *Phys Fluids,* vol. 27, p. 052004.

Wang Z M, Wu R G, Wang Z P, Ramanujan R V (2016), "Magnetic Trapping of Bacteria at Low Magnetic Fields," *Sci Rep,* vol. 6, p. 26945.

Ward K, Fan Z H (2015), "Mixing in microfluidic devices and enhancement methods," *Journal of Micromechanics and Microengineering,* vol. 25, 094001.

Yi C Q, Li C W, Ji S L, Yang M S (2006), "Microfluidics technology for manipulation and analysis of biological cells," *Analytica Chimica Acta,* vol. 560, pp. 1-23.

Zakinyan A, Mkrtchyan L, Dikansky Y (2016), "Experimental investigation of surface instability of a thin layer of a magnetic fluid," *European Journal of Mechanics-B/Fluids,* vol. 56, pp. 172-177.

Zeng J, Deng Y, Vedantam P, Tzeng T-R, Xuan X (2013), "Magnetic separation of particles and cells in ferrofluid flow through a straight microchannel using two offset magnets," *Journal of Magnetism and Magnetic Materials,* vol. 346, pp. 118-123.

Zhu G P, Nguyen N T (2012a), "Magnetofluidic spreading in microchannels," *Microfluidics and Nanofluidics,* vol. 13, pp. 655-663.

Zhu G P, Nguyen N T (2012b), "Rapid magnetofluidic mixing in a uniform magnetic field," *Lab on a Chip,* vol. 12, pp. 4772-80.

Zhu T, Cheng R, Lee S A, Rajaraman E, Eiteman M A, Querec T D, Unger E R, Mao L (2012c), "Continuous-flow ferrohydrodynamic sorting of particles and cells in microfluidic devices," *Microfluidics and Nanofluidics,* vol. 13, pp. 645-654.

Zolgharni M, Azimi S M, Bahmanyar M R, Balachandran W (2007), "A numerical design study of chaotic mixing of magnetic particles in a microfluidic bio-separator," *Microfluidics and Nanofluidics,* vol. 3, pp. 677-687.